Journal of the Meteorological Society of Japan, Vol. 92, No. 4, pp. 327–346, 2014
DOI:10.2151/jmsj.2014-404

Spatio-Temporal Variation of High-Temperature Events in Hokkaido, North Japan

Keisuke MORI

Graduate School of Environmental Science, Hokkaido University, Sapporo, Japan

and

Tomonori SATO

Faculty of Environmental Earth Science, Hokkaido University, Sapporo, Japan

(Manuscript received 7 November 2013, in final form 18 April 2014)

Abstract

This study investigated the spatiotemporal characteristics of high-temperature events in Hokkaido, Japan, using observational data of 26 years. Statistical analyses revealed that the annual mean frequency of these events was lower (higher) at stations on the western (eastern) side of Hokkaido. The frequency of these events showed clear seasonal variation with two distinct peaks occurring in January and May. In addition, the local time of the high-temperature onset was strongly dependent on the season; the onset occurred more frequently from 1600 to 0400 Japan Standard Time (JST) in January and from 0700 to 1300 JST in May.

The seasonal dependence mechanism of the high-temperature onset was investigated in eastern Hokkaido, where the frequencies of both January and May high-temperature events were the highest. In January, an extratropical cyclone passage caused intensified warm advection and increased precipitable water vapor, leading to weakened radiative cooling during the night. In May, the high-temperature events were triggered by two different mechanisms related to solar insolation. The first mechanism is explained by dynamic foehn, which forms the subsidence of the high potential temperature layer on the lee of mountains. However, the nocturnal inversion layer prevented vertical mixing of the foehn-induced warm air aloft and cold air near the ground. The surface air temperature dramatically increased after sunrise when the nocturnal inversion layer disappeared. The second mechanism is explained by the combination of airflow diabatically heated by surface sensible heat flux and dynamic foehn. Therefore, solar insolation is the key factor that controlled the diurnal variation in high-temperature events in May.

Keywords Foehn; high temperature; diurnal variation; solar radiation

1. Introduction

Surface air temperature has prominent diurnal and seasonal cycles in accordance with solar radiation intensity. Such regular variations in surface air temperature are occasionally modified because of various atmospheric phenomena. The spectrum of surface air temperature exhibits a peak corresponding to the frequency of synoptic-scale disturbances as well as those of annual and diurnal cycles (Monin and Yaglom 1975). Because the dominant synoptic-scale pressure pattern is strongly dependent on the season, the frequency of anomalous temperature events is expected to vary among seasons. Synoptic-scale disturbances induce mesoscale circulations that influence local-scale temperature distribution (Orlanski 1975).

Mesoscale atmospheric processes modify temperature variations on a local scale. In particular, many

Corresponding author: Keisuke Mori, Graduate School of Environmental Science, Hokkaido University, Kita-10, Nishi-5, Sapporo, Hokkaido 060-0810, Japan
E-mail: kei_m0221@ees.hokudai.ac.jp

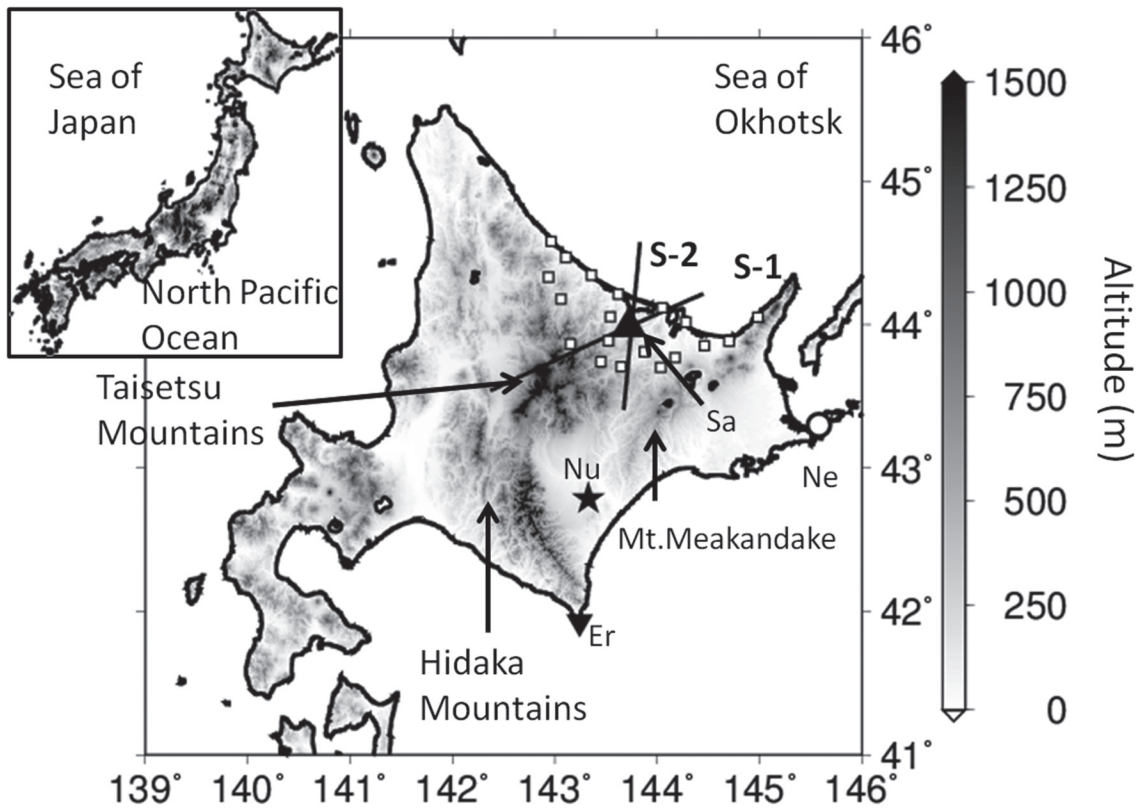

Fig. 1. Topography near Hokkaido, Japan. White squares indicate the stations in the Okhotsk area. The black triangle represents Saroma station (Sa; 43.98°N, 143.72°E). The black inverted triangle represents Erimo-misaki station (Er; 41.92°N, 143.24°E). The white circle represents Nemuro station (Ne; 43.3°N, 145.58°E). The black star represents Nukanai station (Nu; 42.78°N, 143.32°E). Lines labeled S-1 and S-2 represent cross sections shown in Fig. 11 and Fig. 12, respectively. Shading represents the topography (m).

studies have sought to reveal the role of orographic forcing (Oard 1993; Raphael 2003; Gaffin 2007; Mayr et al. 2007; Lin 2007; Ishizaki and Takayabu 2009; Markowski and Richardson 2010) and horizontal convection (Fujibe 1999a; White 2009; Markowski and Richardson 2010; Nallapareddy et al. 2011) in amplifying the temperature variations.

Orographically forced local circulations tend to exhibit seasonal variations caused by seasonal changes in synoptic-scale pressure patterns. Near the Appalachian Mountains in North America, approximately two-thirds of the foehn events occurred during November to April (Gaffin 2007), suggesting that foehn events have strong seasonality and peak during the cold season. In the Toyama Plain, Japan, Ishizaki and Takayabu (2009) showed seasonal variations in sudden warming events with maximum frequencies occurring in March and April. Furthermore, Fujibe (1999a) and Mayr et al. (2007) reported that numerous warming events occur during a specific time of the day, indicating that the occurrence of a high-temperature event is strongly related to the diurnal cycle.

Hokkaido Island, located in northern Japan, comprises a complex terrain, with the Taisetsu Mountains in the center (Fig. 1). Because Hokkaido is located within the zone of prevailing westerlies, traveling cyclones periodically pass in its vicinity (Asai et al. 1988; Chen et al. 1991; Hayasaki and Kawamura 2012). Therefore, the roles of mesoscale circulation induced by synoptic disturbances such as foehn wind, land–sea breeze circulation, and gap flow in triggering rapid temperature change have been investigated in Hokkaido (Arakawa 1969; Nagasawa and Miyagawa 1980; Ikawa and Nagasawa 1989; Fujibe 1999a). Because a majority of previous

research consisted of case studies, climatological features of high-temperature events, such as seasonal cycles and mean diurnal variations, remain unclear. In addition, the spatial distribution of these events in relation to the topography in Hokkaido remains unknown. High-temperature events have strongly influenced natural events such as the triggering of snowslides during late winter to early spring (Matsushita et al. 2012). Therefore, it is necessary to understand the mechanism of high-temperature events induced by orographic effects.

This study aims to clarify the temporal and spatial variations of high-temperature events in Hokkaido. To achieve this objective, statistical analyses of these events were conducted using observational surface air temperature data. Furthermore, to elucidate the physical mechanism responsible for temporal variation in high-temperature events, detailed analyses of typical high-temperature events were conducted.

The outline of the paper is as follows: In Section 2, observational data used in statistical analyses, including definitions of high-temperature events, are described and the results are presented in Section 3. In Section 4, environmental conditions during high-temperature events based on case studies are shown and the conclusions are presented in Section 5.

2. Methodology and data

Statistical analyses were conducted using hourly surface air temperature data observed by 155 stations of the Automated Meteorological Data Acquisition System network operated by the Japan Meteorological Agency from 1984 to 2009. In this study, high-temperature events were selected according to the following procedure. First, 7-day running mean temperature $\overline{T}(t, t = 1, 24)$ was computed for each local time t. $\overline{T}(t)$ corresponds to the mean diurnal variation in original temperature $T(t)$ over a 7-day period that included the target day and three days before and three days after. Second, the anomaly of the observed temperature $T'(t)$ was calculated as a deviation of $\mathrm{T}(t)$ from $\overline{T}(t)$. Because this process functions as a high-pass filter, it allows us to focus on the temperature fluctuation caused by mesoscale weather phenomenon, regardless of trends over a week. Third, high-temperature events were detected when $T'(t)$ exceeded the threshold value of 4.77, which corresponds to an average of 95th percentiles for $T'(t)$ from 1984 to 2009 at each station; the 95th percentile values range from 3.01 to 6.14. The use of a constant threshold enabled us to determine the spatial distribution of occurrence frequency among areas in which high-temperature events occur. The local time at which $T'(t)$ first exceeds the threshold value during a continuous event is defined as initial time. Finally, to avoid multiple detections of one continuous event, statistical analysis was conducted only for high-temperature events exceeding 4 h, which corresponds to the mode for medians of duration for all such events at each station.

3. Statistical analyses

3.1 Seasonal and diurnal variations in high-temperature events

Figure 2 shows seasonal variations in the frequency of high-temperature events for the entire area of Hokkaido. The frequency of high-temperature events was greater than 3 month^{-1} in fall (September to November), winter (December to February), and spring (March–May). The highest and lowest frequencies were detected in January and summer, respectively. Seasonal variations in high-temperature events appeared to be similar to annual variations in the monthly mean frequency of cyclones crossing the longitude of 140° E in the latitudinal belt between 20° N and 56° N indicated by Asai et al. (1988), which showed that cyclones pass less frequently in summer than in other seasons.

The duration of high-temperature events indicated a distribution similar to exponential distribution. The median of durations ranged from 8 to 10 h at each station, the mode of which was 9 h. Long-duration events of at least 24 h tended to be observed in winter than in other seasons (figure not shown). These events accounted for fewer than 6 % of all events in a given month.

Diurnal variation in the initial time of high-temperature events is shown in the lower panel in Fig. 2. In January and May, the frequency was high from 1600 Japan Standard Time (JST = UTC + 0900) to 0400 JST and from 0700 JST to 1300 JST, respectively. The initial time of the high-temperature events was classified into two types with respect to season: that from fall to early spring (March) is referred to as the winter type and that from early spring (April) to early summer (July) is referred to as the spring type. In the winter and spring types, the frequencies in January and May were the highest, respectively. Two transitional periods were noted in March–April and October–November, both of which exhibited one diurnal peak in the evening similar to that in the winter and one in the morning similar to that in the spring. Thus, the initial time exhibited a distinct seasonal change. From January to April, the frequency

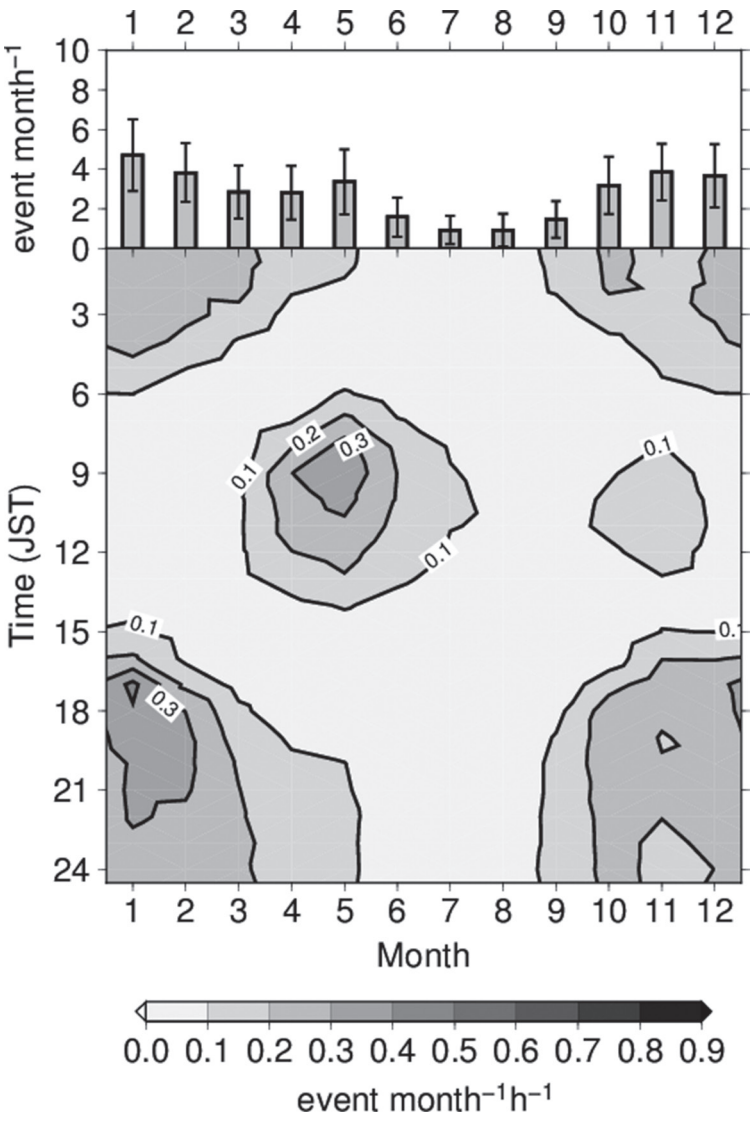

Fig. 2. Diurnal and seasonal variation in high-temperature event frequency for 155 stations in Hokkaido. Upper panel represents monthly average frequency of high-temperature event (event month^{-1}). Lower panel represents monthly (lateral axis) and diurnal (vertical axis) variations in the high-temperature event occurring at a particular time of the month (event month^{-1} h^{-1}).

of high-temperature events that occurred from evening to early morning decreased in accordance with the increased frequency of events occurring from morning to noon.

3.2 Spatial distribution

Figure 3 illustrates the spatial distribution of the annual mean frequency of high-temperature events in Hokkaido and the monthly mean frequency in January and May, which showed higher values than those in other months. The average frequency was lower at stations on the western side of Hokkaido than those on the eastern side throughout the year. The highest annual frequency of high-temperature events (59.2 events yr^{-1}) was observed at Saroma station (black triangle in Fig. 1). The lowest annual occurrence frequency (5.5 events yr^{-1}) was observed at Erimo-misaki station (black inverted triangle in Fig. 1).

The highest frequency in January was 9.3 events

month^{-1} observed at Nukanai station (black star in Fig. 1), which is located in an inland basin (Fig. 3b). The average frequency of high-temperature events in January was higher inland than at coastal stations. This result probably reflected the varying intensity of nocturnal radiative cooling between land and ocean and the large heat capacity of the ocean, which caused milder temperature variations in coastal areas than those inland.

In May, the frequency of high-temperature events was higher in the Okhotsk area relative to other areas. The highest frequency was found at Saroma station (6.4 events month^{-1}). The high-temperature frequency differed significantly between the eastern and western sides of the Hidaka Mountains. The frequency was higher on the eastern side of the mountain, where the downslope wind is dominant in the lower troposphere, as shown in Section 4. The frequency of high-temperature events was remarkably lower on the windward, or western, side of the mountain, showing a west-low east-high pattern. A similar contrasting feature in foehn frequency was observed near the Appalachian Mountains, where higher frequencies appeared on the downwind side of the seasonally varying prevailing winds (Gaffin 2007).

4. Environmental conditions during high-temperature events

In this section, the physical mechanisms of high-temperature events in the Okhotsk area (Fig. 1) were investigated for January and May, when the occurrence frequencies were high (Fig. 3). As shown in Fig. 4, the characteristics of seasonal and diurnal variations in high-temperature frequencies in the Okhotsk area were similar to those observed in the entire Hokkaido region (Fig. 2). Because the local time of the maximum frequency differed between January and May, the formation mechanisms of high-temperature events were expected to vary between months. Thus, January and May are discussed separately in Sections 4.1 and 4.2, respectively. The analysis was targeted for the high-temperature events observed at Saroma station (Fig. 1). To focus on the most typical events, the high-temperature events that occurred during 1600–0100 JST in January and 0600–1300 JST in May were examined when the highest frequency appeared in the statistical analysis (Fig. 4).

4.1 January

High-temperature events in January were most frequently observed during 1600–0100 JST, with 167 events recorded during 1984–2009 (Fig. 4). In this section, we will examine how atmospheric conditions during the high-temperature events are different from those in climatology. Figure 5 represents the statistics of lower tropospheric temperature advection (Appendix A) and precipitable water vapor (Appendix B) during 1984–2009. The 1000-hPa level temperature advection at 2100 JST was computed using grid points near Saroma with 6-hourly JRA-25 reanalysis data (Onogi et al. 2007) on 1.125° grids. Precipitable water vapor was computed by radiosonde sounding at 2100 JST in Nemuro station (Ne; white circle in Fig. 1). The cumulative probability distribution of temperature advection indicates stronger warm advection during high-temperature events than that on days without such events (Fig. 5a), which is statistically significant ($p < 0.01$) according to the Wilcoxon rank sum test. A second analysis indicated that the cyclone centers were located near Japan (30°–60° N and 120°–160° E) in approximately 50 % of the 167 events in January (figure not shown). This supports the fact that synoptic-scale circulation is mainly attributed to warm advection in relation to the passage of cyclones, which triggers high-temperature events during the cold season.

Because high-temperature events in January were characterized by their high occurrence frequency during the night, some additional factors other than synoptic-scale warm advection appear to be necessary for explaining local time dependency. Figure 5b shows the probability distribution of precipitable water vapor at 2100 JST. The amount of precipitable water vapor during the high-temperature events tended to be larger than that without such events (statistically significant with a 99 % confidence level, confirmed by the Wilcoxon rank sum test). During the night, radiative cooling in the surface layer was weakened because of increased emission–absorption of infrared radiation in the case of enhanced atmospheric water vapor. Therefore, the amount of water vapor is an important factor for explaining the night-time high frequency observed in the cold season. This analysis indicates only the effect of water vapor; however, the role of cloud cover for moderating radiative cooling is also an important factor. It is suggested that the high-temperature events were formed by warm advection and increase in downward long-wave radiation, which prevented strong cooling during the night and became increasingly important in the cold season.

Here we provide two examples of high-temperature events observed on January 13, 2000 and January 6, 2005 in order to explain the spatiotemporal varia-

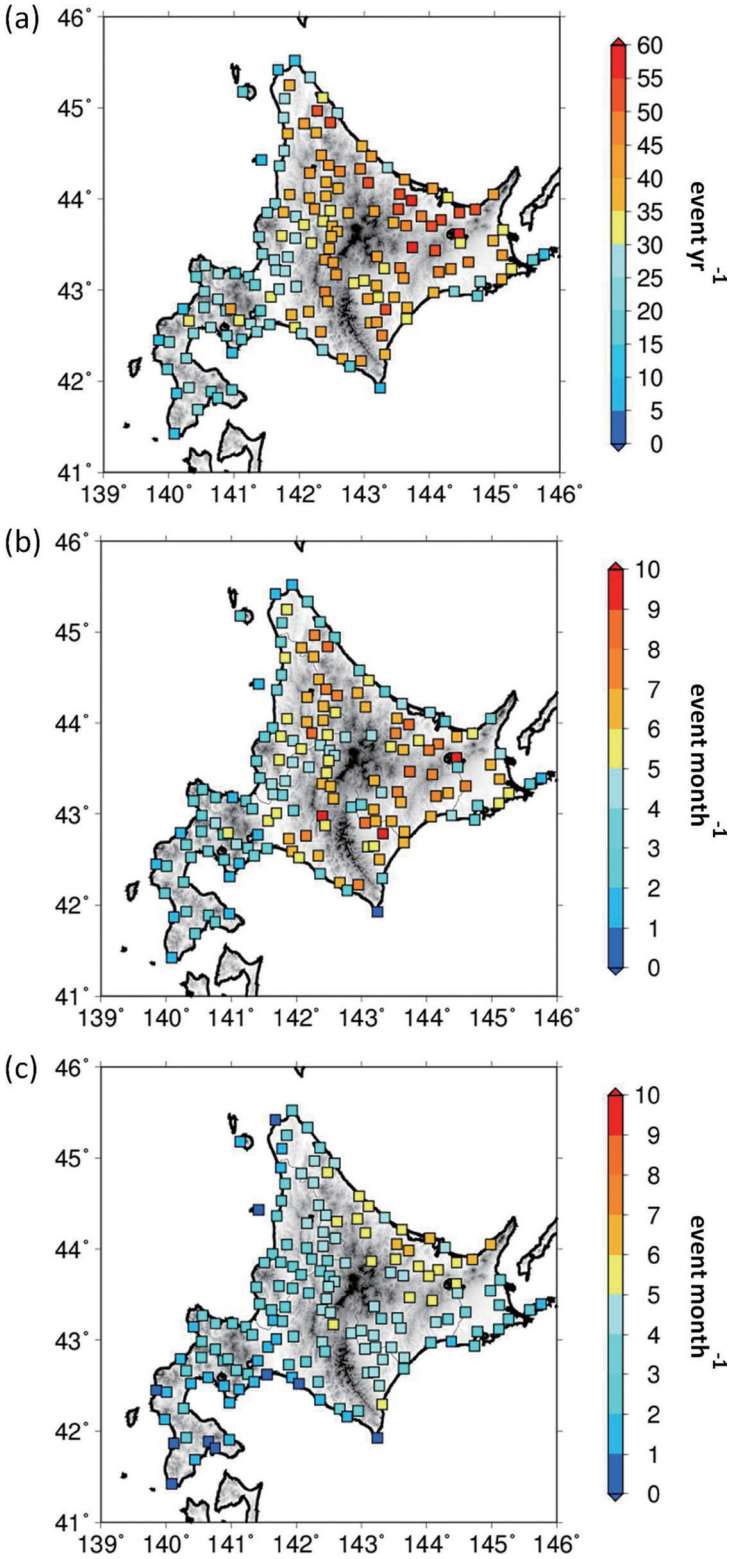

Fig. 3. Horizontal distribution of high-temperature event frequency in Hokkaido. (a) Annual mean (event yr^{-1}); (b) January (event $month^{-1}$); and (c) May (event $month^{-1}$).

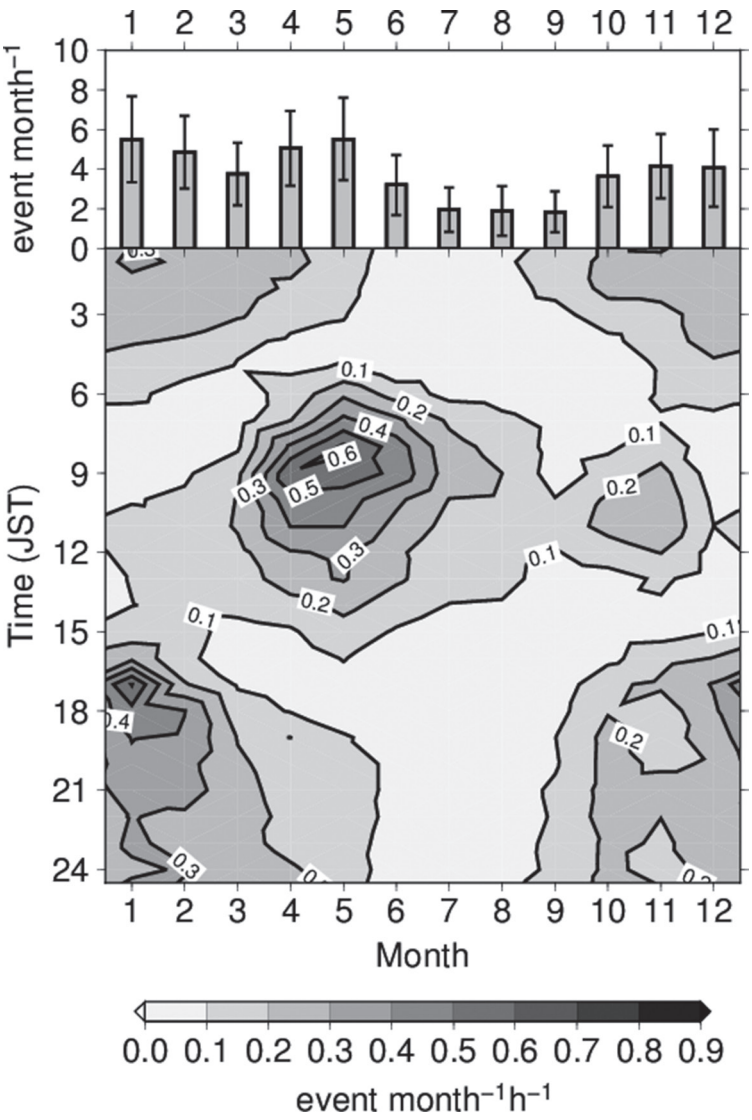

Fig. 4. Same as Fig. 2, but for the Okhotsk area.

tion in the high-temperature events in January. The former event indicates the role of a large amount of precipitable water vapor and the latter indicates the role of warm advection. Figure 6 indicates the observed hourly temperature, wind direction, wind speed, and 7-day running mean diurnal variation in temperature $\overline{T}$. The diamond in Fig. 6 shows the temperature advection corresponding to the grid point in Saroma at 1000 hPa calculated using 6-hourly JRA-25 reanalysis. The first high-temperature event continued during a 16-h period from 1800 JST on January 13, 2000 to 1000 JST on January 14, 2000. The temperature on January 13 did not decrease in the late afternoon although the running mean temperature $\overline{T}$ began to decrease after 1500 JST, according to the decrease in solar insolation. The amount of precipitable water vapor in January 13, 2000 was the highest (20.24 mm) in the same month during 1984–2009 (figure not shown). Warm advection was dominant throughout the event except for a period of weak cold advection in 2100 JST. The weather chart at 2100 JST showed an extratropical cyclone located near central Japan that caused southerly to easterly winds over eastern Hokkaido (Fig. 7a), which maintained the warm advection. Furthermore, the satellite images indicated dense cloud coverage over Hokkaido

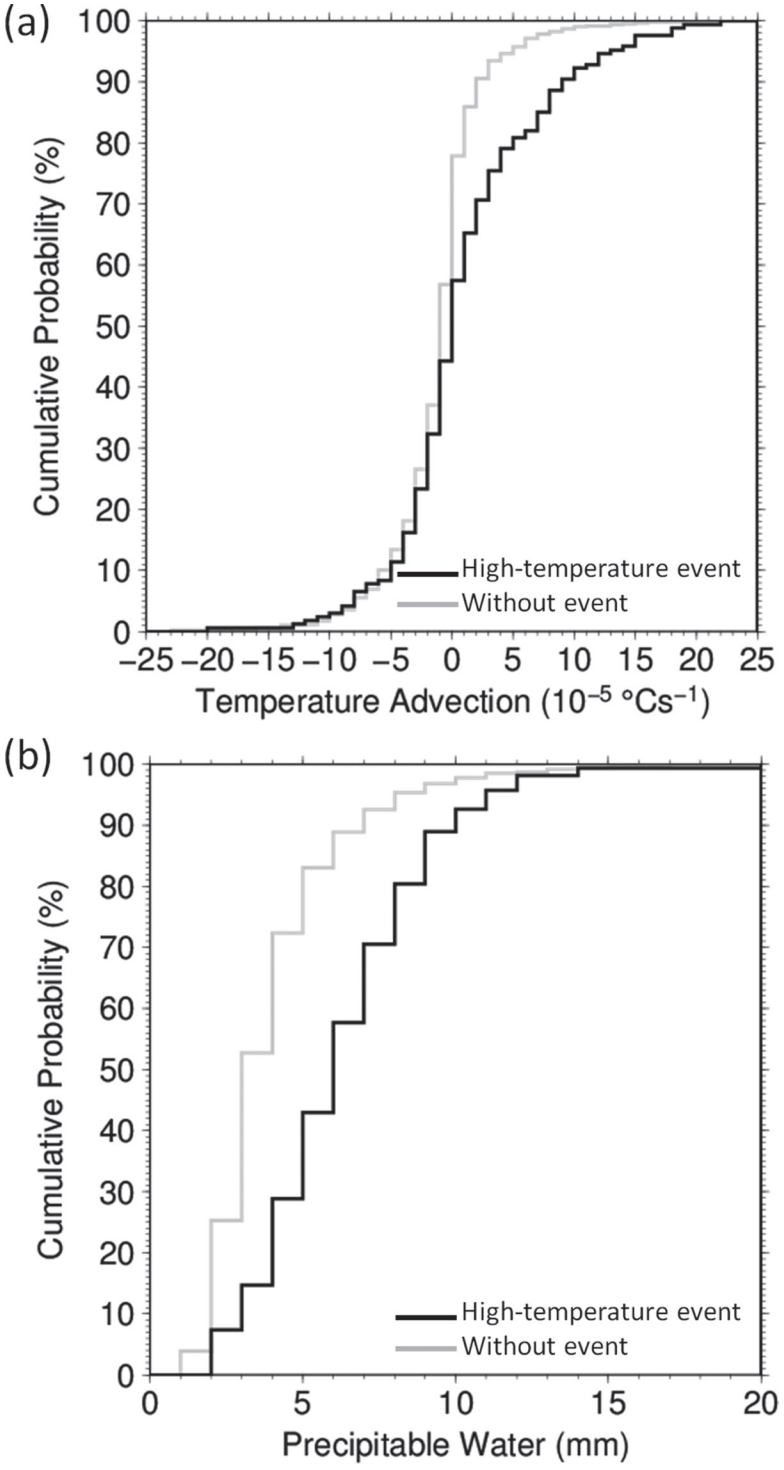

Fig. 5. Cumulative probability distribution of (a) the temperature advection calculated by 6-hourly JRA-25 reanalysis (positive indicates warm advection) and (b) precipitable water vapor at 2100 JST in January observed at Nemuro station during 1984–2009. The gray line represents cumulative probability at 2100 JST in January during 1984–2009, except for the high-temperature events of January. The black line illustrates cumulative probability at 2100 JST in the high-temperature events of January.

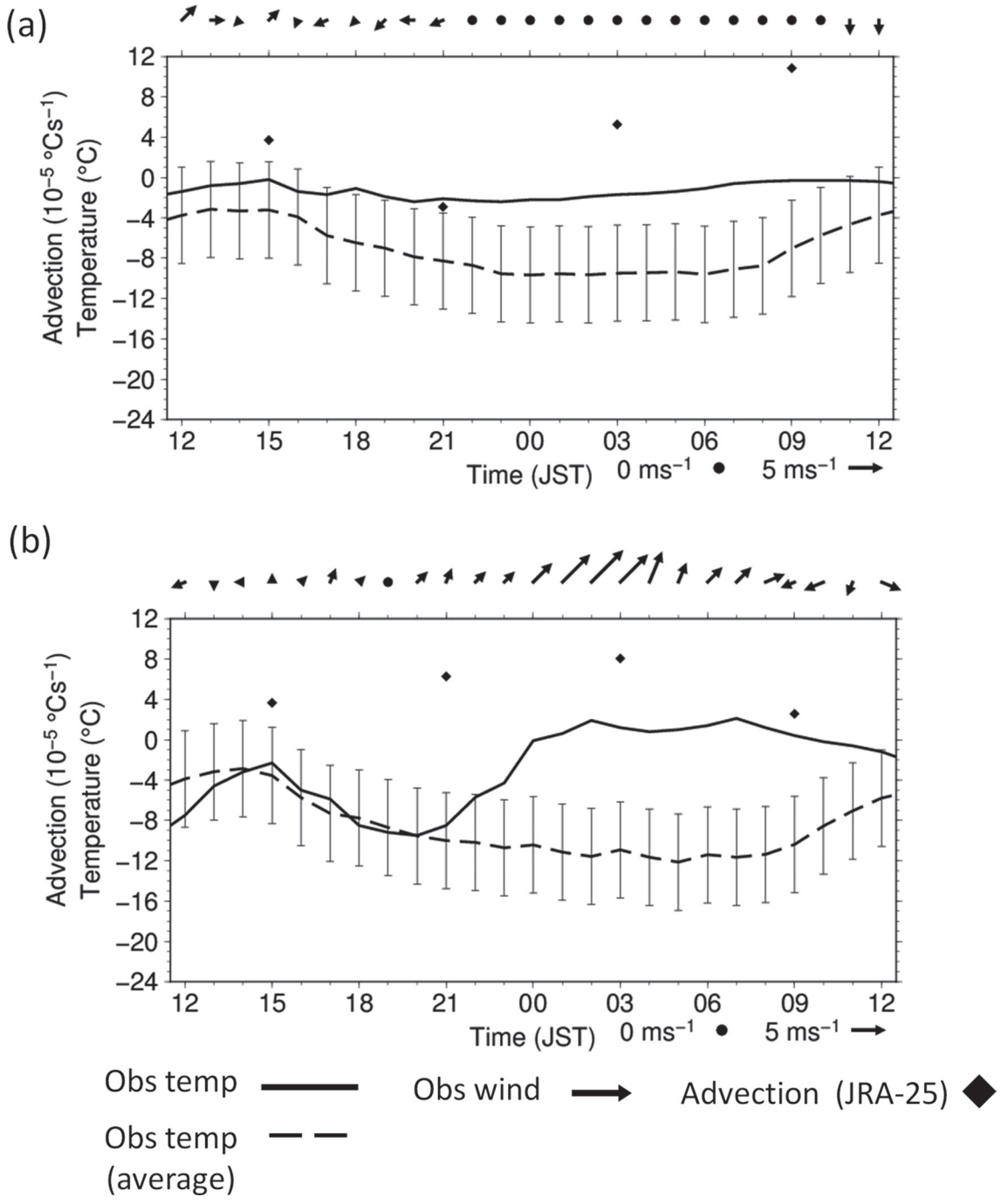

Fig. 6. Time series of surface air temperature (solid line), and 7-day running mean temperature (dashed line) observed at Saroma station. Error bars depict ±4.77 °C (the mean of 95 percentiles for anomalies of each station). Vectors represent surface wind observed at Saroma. Diamonds indicate temperature advection calculated by 6-hourly JRA-25 reanalysis. High-temperature events occurring on (a) January 13–14, 2000 and (b) January 6–7, 2005 are shown.

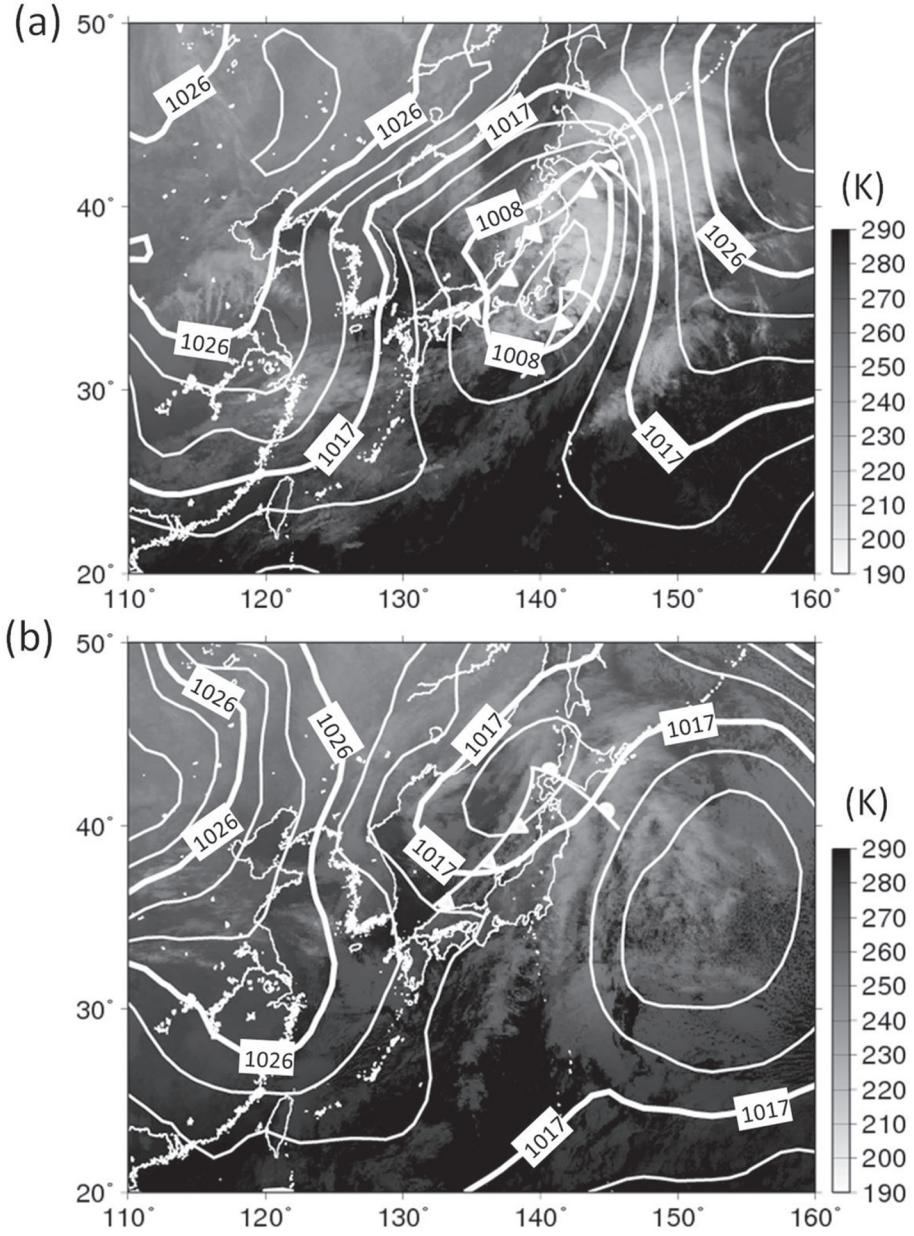

Fig. 7. Surface weather maps with isobars (hPa) determined using JRA-25 and infrared images captured by geostationary satellites at (a) 2100 JST on January 13, 2000, derived from the IR1 channel (10.3–11.3 μm) of GMS, and at (b) 2100 JST on January 6, 2005, derived from the IR1 channel (10.2–11.2 μm) of GOES-9. Shading represents black-body temperature (K).

in association with the cyclone, which would further inhibit a decrease in temperature after sunset by absorbing the infrared radiation emitted from the surface layer.

The second high-temperature event shown here was detected during a 13-h period from 2300 JST on January 6, 2005 to 1100 JST on January 7, 2005. The warm advection at 2100 JST on January 7 was determined to be the strongest among the 167 January events observed in the Okhotsk area. A rapid temperature increase was observed after 2000 JST, whereas the running mean temperature continued to decline

Table 1. Physics schemes of the Weather Research and Forecasting (WRF) model used in this numerical experiment.

	Physics	Reference
Cloud Microphysics	Kessler scheme	Kessler (1969)
Longwave Radiation	RRTM scheme	Mlawer et al. (1997)
Shortwave Radiation	Dudhia scheme	Dudhia (1989)
Surface Layer	Nakanishi and Niino PBL's surface layer scheme	Nakanishi and Niino (2004)
Land Surface	Noah Land Surface Model	Chen and Dudhia (2001)
Planetary Boundary layer	Mellor-Yamada Nakanishi and Niino Level 2.5 PBL	Nakanishi and Niino (2004)
Cumulus Convection	Grell scheme	Grell and Devenyi (2002)

after 1500 JST, which resulted in the increased temperature anomaly T' and the high-temperature event that began at 2300 JST (Fig. 6b). $T'(t)$ dramatically increased after 2100 JST as the southwesterly wind intensified, which is in good agreement with the intensified warm advection recorded during 2100–0300 JST. Figure 7b indicates a low-pressure system centered over the northern Sea of Japan to the west of Hokkaido at 2100 JST, January 6, 2005. Therefore, strong southwesterly winds that brought warm advection were caused by cyclonic circulation due to the low-pressure system. Figure 7b also indicates the weakening of the evening cooling because of dense cloud coverage over Hokkaido, in association with the passage of the cyclone.

Atmospheric conditions during the high-temperature events in January are summarized in the following manner: Warm advection prevailed during the passage of cyclones, which worked to prevent a rapid temperature drop after sunset. Dense cloud coverage and abundant precipitable water vapor caused by a cyclone passage weakened cooling more efficiently during night time than during daytime because long-wave radiation is a dominant factor for determining surface energy balance after sunset (Groen 1947; Iijima and Shinoda 2002). Thus, high-temperature events in winter are likely to form during the night when cyclones approach Hokkaido, which prevents a decrease in nocturnal temperature (Fig. 6a) or a rapid increase in night-time temperature (Fig. 6b). The mechanical effect of strong winds, which occasionally breaks the surface inversion layer, is an additional factor in night-time high-temperature events (White 2009; Kusaka et al. 2011). In the case of January 13, 2000, however, the wind speed was not strong at Saroma (Fig. 6a). Therefore, it is suggested that the breakup of the nocturnal inversion layer is not always necessary for the occurrence of high-temperature events near Okhotsk area in winter.

4.2 May

High-temperature events in May were most frequently observed during 0600–1300 JST (Fig. 4) among the 109 events detected from 1984 to 2009 near Okhotsk area. Because high frequency was detected over the lee, or eastern, side of the mountain (Fig. 3c), the orographic effect is important for high-temperature events in May. Additionally, solar insolation may have played a role in determining the high frequency in morning hours (Fig. 4). However, it is difficult to discuss the orographic effect on the basis of the available surface observations. Therefore, we conducted numerical experiments using a regional atmospheric model to investigate the roles of solar insolation and topography on the occurrence of high-temperature events in May.

We used the Weather Research and Forecasting (WRF) model version 3.2.1 with the Advanced Research WRF dynamical core (Skamarock et al. 2008). The domain of the numerical simulation was 192 × 172 grids at 5-km intervals centered at 43° N and 142° E. The WRF has 32 levels with a sigma coordinate, and the model top was set to 50 hPa; Table 1 presents the physical scheme of the WRF model. The 6-hourly JRA-25 reanalysis data were used as the initial and lateral boundary conditions. A daily Optimally Interpolated Sea Surface Temperature (Reynolds et al. 2007) was employed for the ocean surface boundary condition.

To investigate the atmospheric motions around the mountains, backward trajectory analysis was conducted using the records of a pre-existing (1984–2009) WRF experiment conducted over Hokkaido with a 10-km mesh size driven with JRA-25 data (Inatsu et al. 2012). Figure 8 displays the passage frequency of backward trajectories of the air parcel that were released from Saroma station for each of the 109 high-temperature events occurring in May. The trajectories were typically divided into two courses before reaching Saroma. The first course (hereafter,

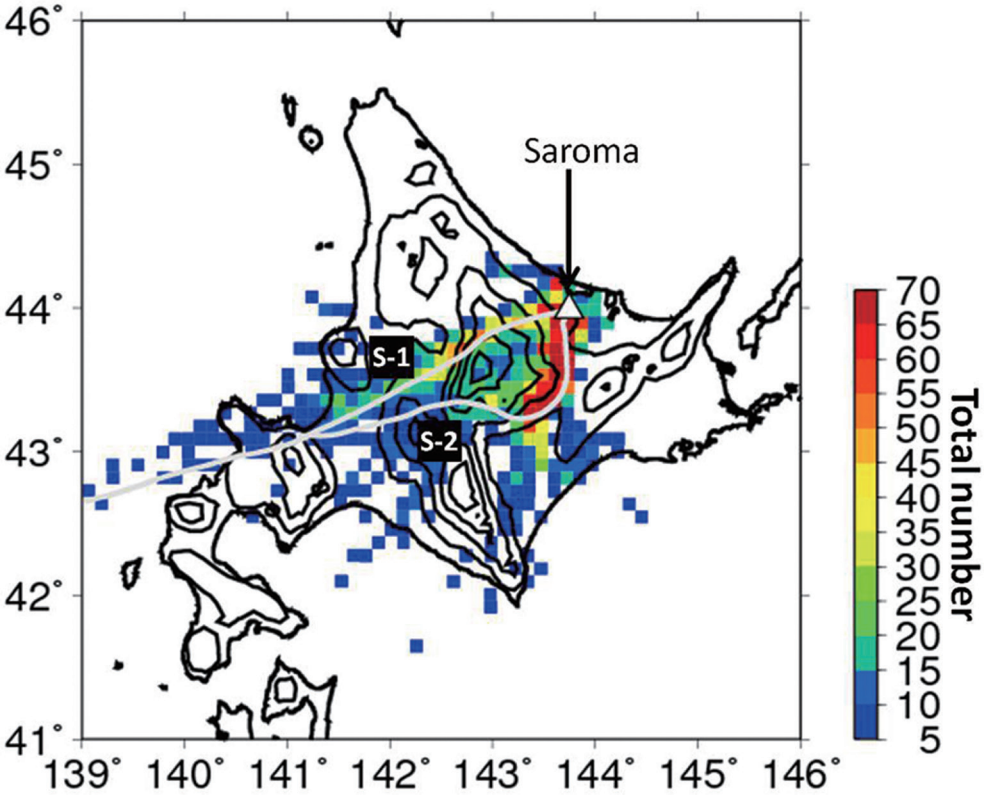

Fig. 8. Passage frequency of the backward trajectories (shading) determined using the 109 high-temperature events of May. Each trajectory was drawn for 12 h prior to the time of high-temperature event occurrence at Saroma. The white triangle represents Saroma station. Lines labeled S-1 and S-2 indicate the backward trajectories in which air parcels were released at 2000 JST on May 16, 1985 and 1900 JST on May 30, 1999, respectively. Contour interval is 250 m of elevation.

S-1 course) runs through the north side of the Taisetsu Mountains and second (hereafter, S-2 course) runs through the gap between the Taisetsu Mountains and Mt. Meakandake. As shown in the figure, two typical high-temperature events on May 17, 1985 and May 31, 1999 were selected to represent S-1 and S-2 courses, respectively. WRF experiments were then conducted with the settings shown in Table 1 (hereafter, S-1-CTL run and S-2-CTL run). The S-1-CTL and S-2-CTL runs were conducted from 0600 JST on May 16, 1985 to 0000 JST on May 18, 1985 and from 0600 JST on May 30, 1999 to 0000 JST on June 1, 1999, respectively.

4.2.1 S-1 course (May 17, 1985)

During the high-temperature event on May 17, 1985, the air parcel took the S-1 course over the north side of the Taisetsu Mountains to reach Saroma station (Fig. 8). No precipitation was recorded near Okhotsk area in the observations on May 17, except at 0300 JST. Solar insolation was observed, beginning at 0500 JST on May 17 at Saroma station. The observed high-temperature event continued for 34 h from 0900 JST on May 17 to 1800 JST on May 18. At Saroma station, the observed surface air temperature increased rapidly over 5 °C every hour from 0600 to 0900 JST (figure not shown). Figure 9 shows the horizontal distributions of surface air temperature and wind field at 0400 JST and 1300 JST in the numerical simulation and observation. Figures 9a and 9b indicate that the high-temperature region is located over the coastal area in the northern part of Hokkaido and that the wind is stronger in the coastal area than inland, at 0400 JST in both the observation and S-1-CTL run. Moreover, surface air temperature greater than 22 °C extends at eastern side of the mountains, and the westerly wind blows at the eastern foot of the Taisetsu Mountains at 1300 JST (Figs. 9a, b). These results

indicate that the S-1-CTL run roughly agrees with the observational data.

Figure 10a shows the center of an anticyclone located in central Japan, in addition to westerly wind covering Hokkaido; thus, Saroma is situated on the lee side of the mountain slope. S-1-CTL indicates air temperatures at 2 and 200 m above ground level (AGL) at Saroma are 1.6 and 8.4 °C respectively at 0400 JST, which suggests that a nocturnal inversion layer developed as a result of cold air accumulation before sunrise (figure not shown).

Figure 11a indicates vertical cross sections along the S-1 line (Fig. 1) in the S-1-CTL run. In S-1-CTL, the air mass with high potential temperature descends on the lee side of the mountain from midnight to early morning. However, the air mass does not penetrate deep into the region of the foot of the mountains before sunrise. A downslope wind exceeding 10 m s^{-1} is present in the shallow layer below 300 m AGL over the lee side of the mountain before 0700 JST. In the vicinity of Saroma, however, the downslope wind is weak, with speeds less than 1 ms^{-1} near the ground. After 0700 JST, the absolute horizontal wind speed near the ground gradually increases and that in the upper layer over the ground weakens, followed by the development of a mixing layer. This suggests that the nocturnal inversion layer at Saroma is diminished by solar insolation after 0500 JST and disappears by 0900 JST. An ascending motion moves from east to west near Saroma from 0700 JST to 1000 JST and west to east from 1000 JST to 1300 JST, which corresponds to the movement of the convergence zone in the lowest layer. Although the pressure gradient suggested westerly geostrophic wind (Fig. 10a), Figs. 9a and 9b show wind convergence occurring in the vicinity of Saroma at 1300 JST. The ascending motion is intensified until late morning; this is similar to the activity of the low-level convergence zone on the lee slope, which showed a distinct diurnal cycle (Fujibe et al. 1999b; Sato and Kimura 2003).

Figure 11a strongly suggests that the high-temperature event on May 17, 1985 is caused by the dynamic foehn. The backward trajectory analysis also suggests that the air parcel that reached Saroma at 0900 JST on May 17 originated 12 h earlier at 1100 m AGL. The subsequent development of a mixing layer enables mixing of the surface cold layer and the high potential temperature layer aloft. As a result, the foehn-derived air mass with high potential temperature is dragged downward, leading to the additional temperature increase in the high-temperature event that is much stronger than expected only because of the surface sensible heat flux. This result is consistent with that reported by Whiteman et al. (1999), which indicates that the upper air temperature condition is strongly related to surface air temperature variation.

A sensitivity experiment was conducted to investigate the role of surface heat flux in breaking nocturnal inversion. The strong downslope wind may have removed the inversion layer, as is known to occur in the Alps during foehn events (Zangl 2003). The experiment followed the settings of S-1-CTL, except for assuming no sensible/latent heat flux from the ground (hereafter, S-1-NoFLX run), in which temporal variation in atmospheric circulation is mainly maintained by the synoptic-scale pressure gradient and topographic effect. In the S-1-NoFLX run, a stronger downdraft (>1 m s^{-1}) occurs at the lee-side slope under 300 m AGL at 1000 JST (Fig. 11b), as shown in the S-1-CTL run (Fig. 11a). However, the downslope wind exhibits very small diurnal variation even after sunrise while maintaining a similar potential temperature structure (Fig. 11b). In both S-1-CTL and S-1-NoFLX, a high potential temperature layer is present in the upper layer because of the dynamic foehn. Therefore, it is inferred that the mechanical effect of the westerly wind in association with the cyclone passage is insufficient for breaking the inversion layer over the foot of the mountains near Saroma. On the contrary, the ground heating by solar insolation and the following turbulent mixing according to the positive sensible heat flux are important factors in removal of the cold air layer that accumulates near the surface. Therefore, solar insolation is necessary for initiating the high-temperature event in May, which is consistent with the fact that high-temperature events most frequently occur in the morning hours (Fig. 4).

4.2.2 S-2 course (May 31, 1999)

This subsection describes the mechanism of high-temperature events that passed through the gap between the Taisetsu Mountains and Mt. Meakandake (S-2 course, Fig. 8). No precipitation was recorded near Saroma station in the observations on May 31, 1999. Sunrise and sunset occurred at approximately 0600 JST and 1800 JST, respectively, at Saroma station. A 9-h high-temperature event was detected on May 31 from 1000 JST to 1800 JST. A temperature increase of more than 2.0 °C h^{-1} was recorded from 0500 to 1000 JST in the observations. After 1000 JST, the temperature changed slowly. The surface temperature and wind conditions in the observations are similar to those in the WRF run at 0400 JST and

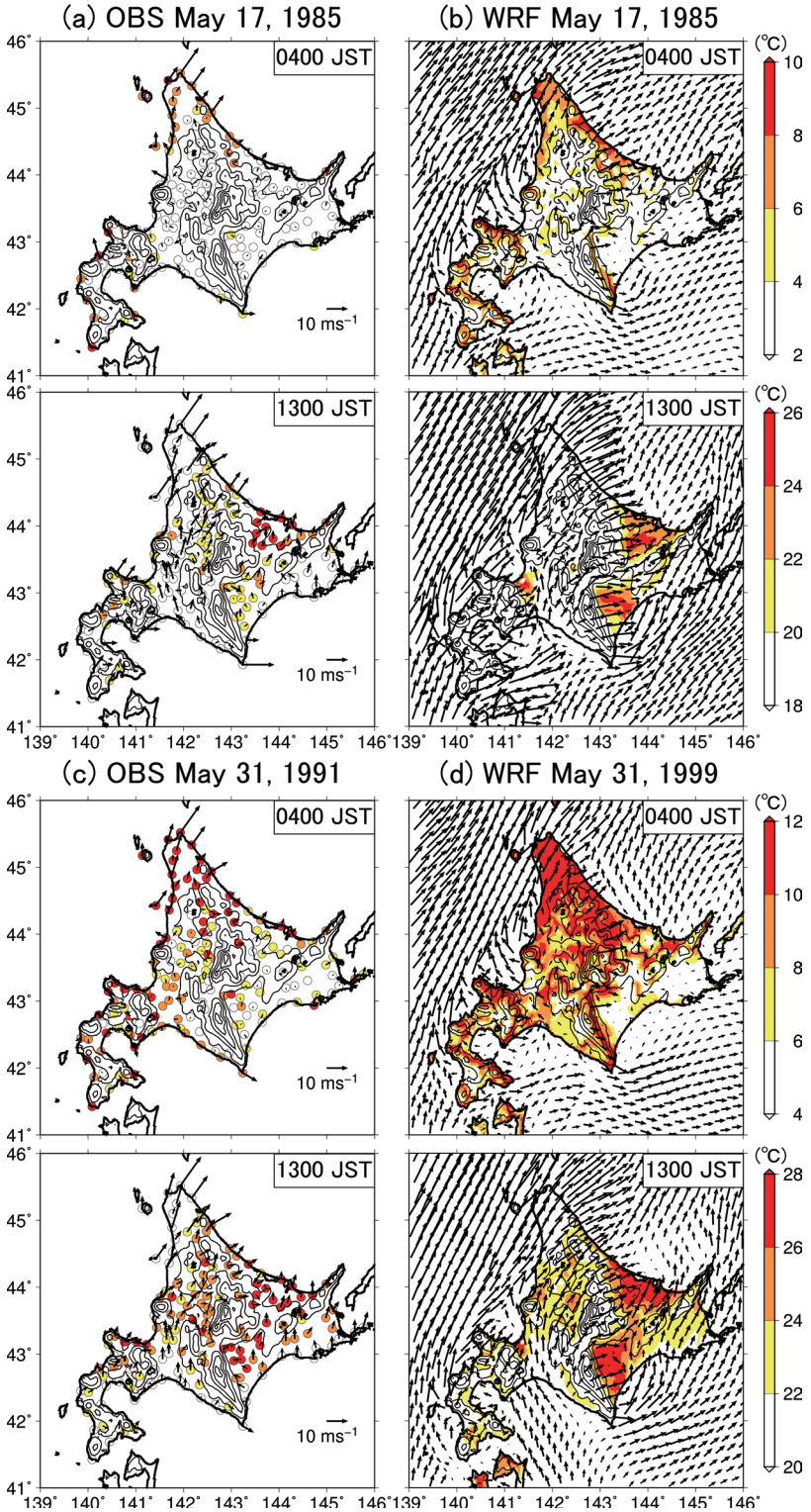

Fig. 9. Surface air temperature (color, °C) and wind field for May 17, 1985 in (a) observation data and in (b) Weather Research and Forecasting (WRF) output for May 31, 1999 in (c) observation and in (d) WRF output. Black vectors represent surface wind. Contour interval is 250 m of elevation.

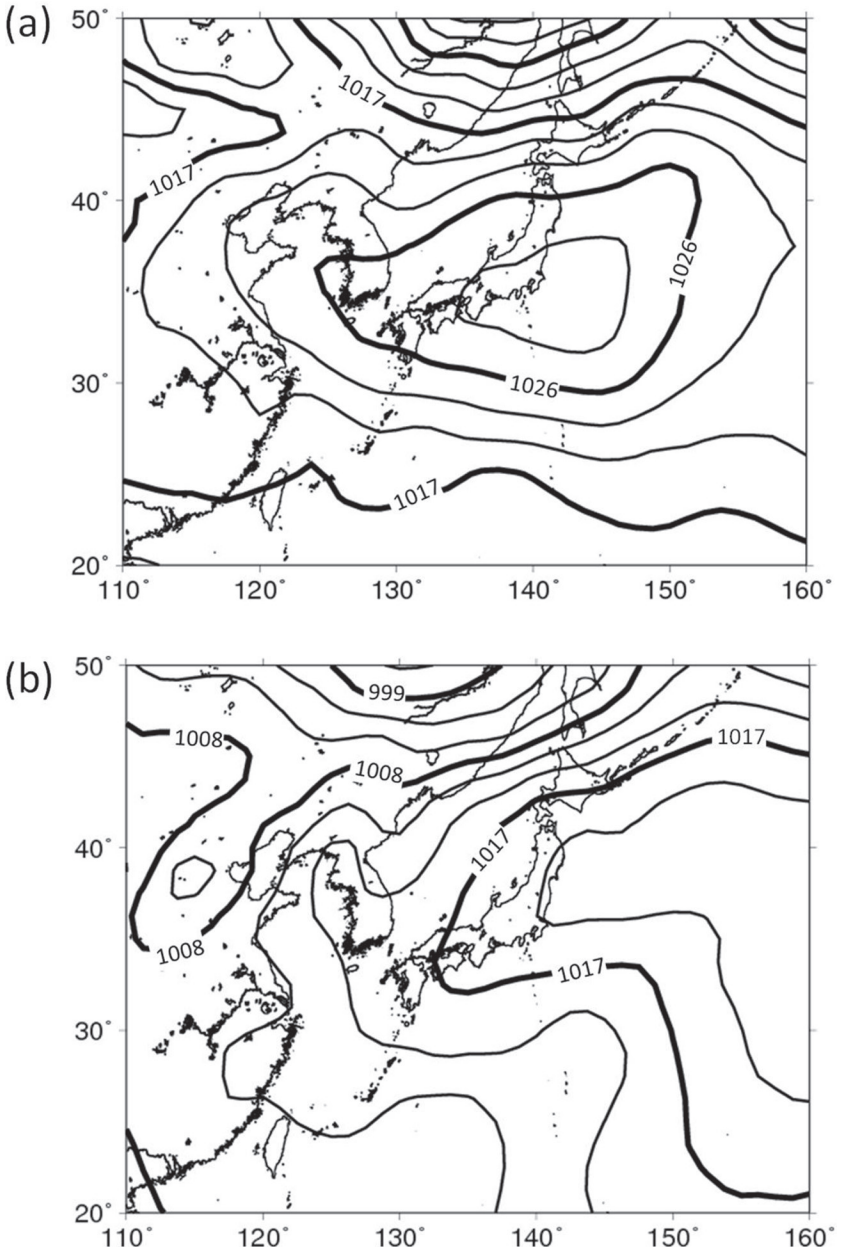

Fig. 10. Maps of surface isobars (hPa) according to JRA-25 data at (a) 0900 JST on May 17, 1985 and (b) 0900 JST on May 31, 1999.

1300 JST, respectively. As shown in Figs. 9c and 9d, a remarkable temperature increase exceeding 20 °C occurs on the lee side of mountains between 0400 JST and 1300 JST. Figure 10b indicates that the center of the anticyclone was located over the southeastern side of Hokkaido and that southwesterly wind prevailed. Saroma is situated on the lee side of mountains.

The nocturnal surface inversion layer present below 95 m AGL at Saroma disappears after 0500 JST (figure not shown). At 0500 JST, the simulated 2 and 95-m temperatures at Saroma are 14.8 and 16.7 °C, respectively, suggesting the accumulation of cold air near the ground. Figure 12 illustrates a time-horizontal cross section of 2-m AGL potential tempera-

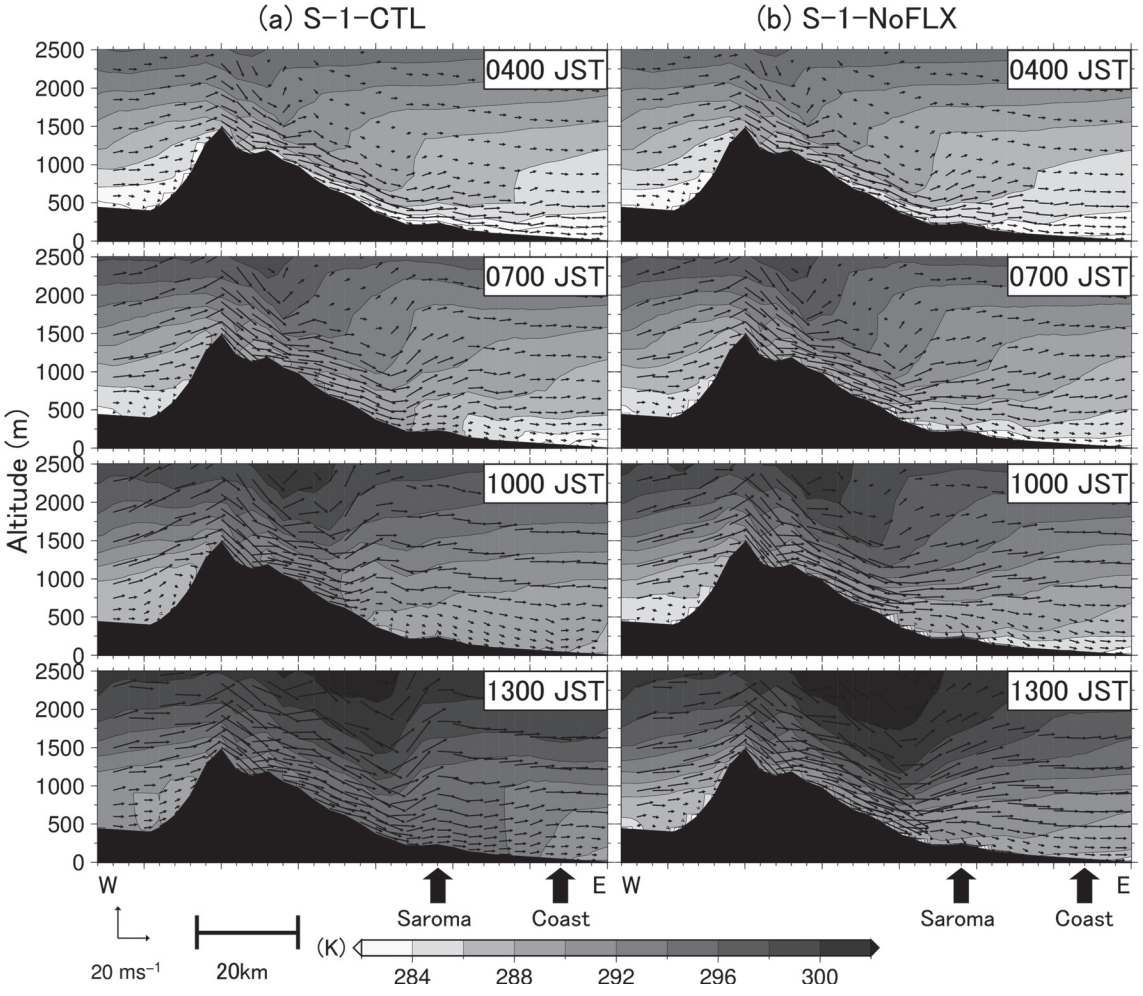

Fig. 11. Vertical cross section of potential temperature on May 17, 1985 along S-1 (Fig. 1) simulated in (a) S-1-CTL and (b) S-1-NoFLX runs. Shading represent potential temperature (K). Vectors represent wind speed and direction along the cross section. Vertical wind is amplified by a factor of 20.

ture and surface winds along the S-2 line (Fig. 1). The horizontal gradient of potential temperature between land and sea is steep to the north of Saroma during 0500 JST–1900 JST on May 31. Although the temperature decreases rapidly during 1700 JST–2200 JST on May 30 in the WRF run, it increases more than 2 °C and is accompanied by intensified wind speed from 2200 JST to 2300 JST on the same day. After 2300 JST on May 30, in the WRF run, the surface air temperature increases slightly during the night. The northward wind, which prevails throughout the day, blows over the southern part of the mountain to the south of Saroma after 0000 JST on May 31. The sea breeze does not penetrate the vicinity of Saroma at noon on May 31. The backward trajectory analysis suggests that the air parcel with a potential temperature of 291.9 K that reached Saroma at 0700 JST on May 31 originated at 270 m AGL, 12 h earlier; these conditions were insufficient for forming the high temperature event. These results indicate that the diabatic heating process by sensible heat flux from the ground warmed by solar insolation is a significant factor for increasing temperature and the dynamic foehn, resulting in the occurrence of high-temperature events. Thus, solar insolation is an essential factor in the high-temperature events taking the S-2 course, which are similar to those in the S-1 course (Subsection 4.2.1). This result indicates that the occurrence of high-temperature events with the S-2 course is also restricted during the daytime.

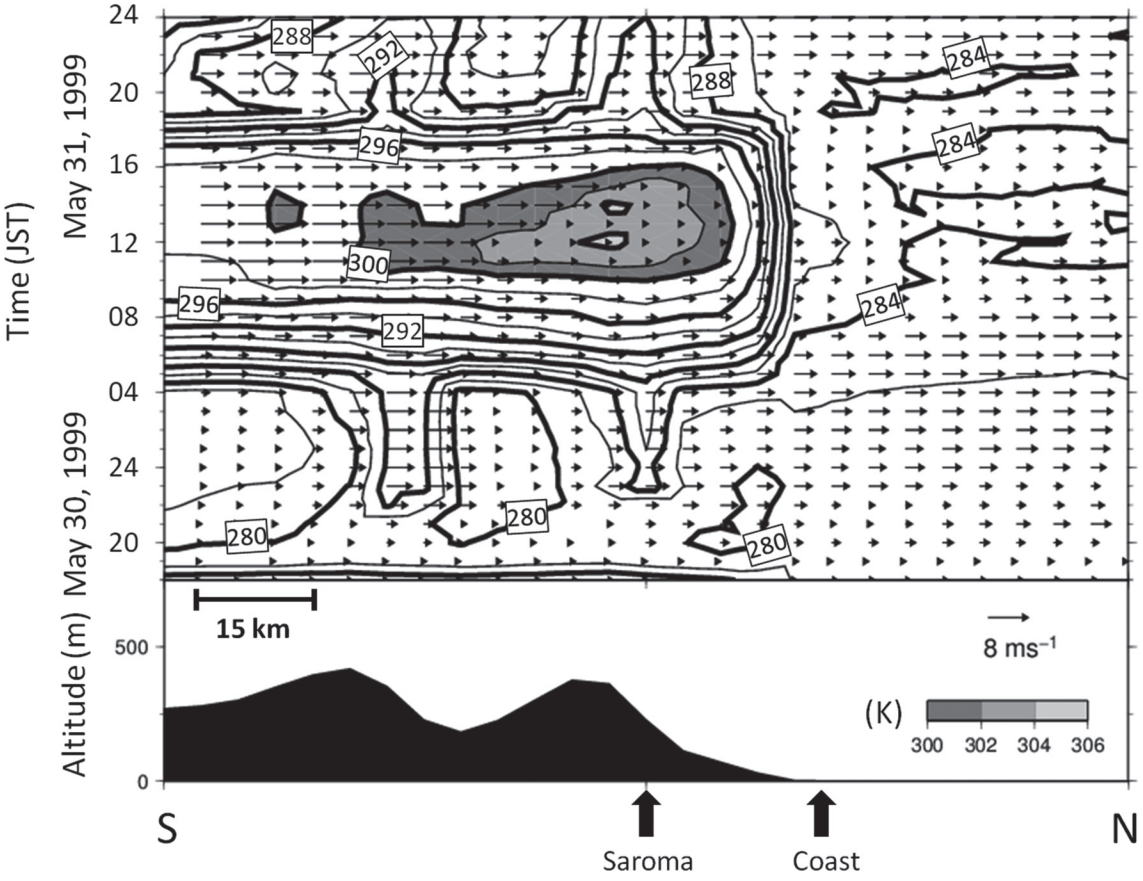

Fig. 12. Time-horizontal cross section of surface potential temperature along the S-2 line (Fig. 1) simulated in the S-2-CTL run. Contour and shading represent surface potential temperature (K). Vectors represent wind vector along the S-2 cross section.

4.2.3 Discussion on the mechanism of high-temperature events in May

According to the backward trajectory analysis, the pathways of air parcels that triggered the high-temperature event in May were classified into two types: one ran along the north side of the Taisetsu Mountains (S-1 course) and the other ran through the gap between the Taisetsu Mountains and Mt. Meakandake (S-2 course). Some high-temperature events occurred as a combination of both types. Thus, the formation mechanism of the high-temperature events over the Okhotsk area is probably explained by a combination of the dynamic foehn and the airflow heated by sensible heat from the ground (Takane and Kusaka 2011). The statistics of the backward trajectory show that the number of high-temperature events taking the S-2 course (approximately 46 % of the total events) was greater than those taking the S-1 course (approximately 35 %). Because the Saroma station is located on the lee side of the gap for the S-2 course and is also on the lee side of the mountain through the S-1 course, this station is the highest-frequency station in Hokkaido. Because precipitation was not observed at the stations located on the backward trajectories from Saroma, the effect of latent heat was not a primary factor for the formation of high-temperature events.

It is suggested that the synoptic-scale pressure pattern, which causes westerly to southerly winds over Hokkaido, is important for foehn phenomena in the Okhotsk area. This is because high-temperature events triggered by the dynamic foehn occurred frequently under a preferable pressure pattern in which an anticyclone was located on the south side of Hokkaido (Fig. 10). This result is similar to that reported in earlier studies (Zangl 2003; Weissmann et al. 2004), which showed that pressure distribution

is an important factor for the occurrence of foehn events in the Alps.

In the S-1-NoFLX run, the cold air is removed mainly by solar insolation so that the high potential temperature aloft is able to descend. A similar effect of solar insolation in breaking the nocturnal inversion layer was reported by Tsunematsu et al. (2005), who showed that vertical momentum mixing that follows surface heating caused an extensive dust outbreak in the morning. In addition, Kondo (1983) determined the intensified surface wind to be the result of momentum exchange in the mixing layer immediately after the inversion breakup by solar insolation, which caused forest fires over the Tohoku district, Japan. In the S-2 course, the high-temperature event does not occur without diabatic heating from the surface sensible heat flux. Because the air parcel passed through the valley, additional energy is available for temperature increase due to heating of the ground and side valley (Egger 1990). Therefore, solar insolation is a key factor for determining the initial times of the high-temperature events.

Although the key factors for controlling the seasonal and diurnal variations in high-temperature events were clarified in this study, the influence of snow cover may have played an additional role in intensifying the temperature anomaly in May. Ikawa and Nagasawa (1989) reported that the dynamic foehn in the Okhotsk area was maintained by airflow over the stable inversion layer formed on the upwind side of the mountain. Therefore, it is important to clarify the effect of snow cover during high-temperature events in the cold season. In addition, the possible effects of sea ice and low sea surface temperature in the Sea of Okhotsk on the high-temperature event in May is a topic for further study because sea ice tends to stabilize the lower atmosphere, resulting in a stronger inversion layer near coastal areas. Thus, further analytical and modeling studies are required, particularly on the relationship between temperature variations and snow cover or sea ice extent.

5. Conclusions

This study aimed to elucidate the spatiotemporal characteristics of the high-temperature events that occurred in Hokkaido, with particular emphasis on seasonal and diurnal variations. A high-temperature event was defined by the temperature deviation from the running mean temperature considering a diurnal cycle. Statistical analyses were conducted using hourly temperature observation data recorded from 1984 to 2009. Detailed analysis and numerical experiments were conducted to determine the mechanism of the high-temperature events. Such analysis provided a quantitative illustration of spatial distribution and seasonal and diurnal variations in the occurrence frequency of high-temperature events.

The findings of this study are summarized in the following points:

1) The frequency of high-temperature events had clear seasonal variation, which showed high frequency from fall to spring and low frequency in summer with two distinguished peaks in January and May. The onset of high-temperature events occurred more frequently from 1600 JST to 0400 JST in January and from 0700 JST to 1300 JST in May.
2) The frequency of high-temperature events showed obvious differences in Hokkaido. The average frequency was lower (higher) at stations on the western (eastern) side of Hokkaido throughout the year; the Okhotsk area showed the highest frequency.
3) The synoptic-scale pressure pattern was an important formation mechanism of the high-temperature events occurring in the Okhotsk area in January. The intensified warm advection and larger amount of precipitable water vapor in association with a cyclone passage led to weakened radiative cooling during the night; therefore, high-temperature events occurred more frequently during the night time than during the daytime.
4) The high-temperature events occurring in May near Okhotsk area were classified into two types depending on the pathways of the air parcels that triggered the events. The first ran over mountains from the west (S-1 course) and the other ran through the gap from the south (S-2 course).
5) The formation factor of the events occurring in the Okhotsk area in May was the dynamic foehn, the airflow heated diabatically by surface sensible heat flux over the mountains or a combination of the two.

This study confirmed that the formation mechanism of typical high-temperature events by dynamic foehn included the following mechanism: The dynamic foehn formed a high potential temperature layer over the cold air above the ground rather than directly penetrating the surface layer, which caused the rapid surface air temperature to increase when vertical mixing was initiated in the surface air after sunrise.

Acknowledgments

This research was supported by the Environment

Research and Technology Development Fund (S-8-1(2)) of the Ministry of the Environment, Japan, the Research Program on Climate Change Adaptation of the Ministry of Education, Culture, Sports, Science and Technology, Japan, and the Grant-in-Aid for Scientific Research on Innovative Areas (25106701) funded by JSPS.

Appendix A

Temperature advection was computed by the central difference method:

$$\frac{\partial T_{i,j}}{\partial t} = -u_{i,j}\frac{T_{i+1,j} - T_{i-1,j}}{2x} - v_{i,j}\frac{T_{i,j+1} - T_{i,j-1}}{2y},$$

where T is the surface air temperature; t is the interval of the JRA-25 dataset (6 h); $\underline{u}$ and v are the zonal and meridional wind speeds, respectively, at 1000 hPa; x and y are the zonal and meridional grid intervals, respectively; and subscripts i and j are the zonal and meridional grid numbers, respectively.

Appendix B

Precipitable water vapor (w_p) is computed by following equation:

$$w_p = -\int_{Psurface}^{Ptop} q_v(p)dp,$$

where q_v is the mixing ratio of water vapor and p is the pressure.

References

Arakawa, S., 1969: Climatological and dynamical studies on the local strong winds, mainly in Hokkaido, Japan. *Geophys. Mag.*, **34**, 349–425.

Asai, T., Y. Kodama, and J. C. Zhu, 1988: Long-term variations of cyclone activities in East Asia. *Adv. Atmos. Sci.*, **5**, 149–158.

Chen, S. J., Y. H. Kuo, P. Z. Zhang, and Q. F. Bai, 1991: Synoptic climatology of cyclogenesis over East Asia, 1958–1987. *Mon. Wea. Rev.*, **119**, 1407–1418.

Chen, F., and J. Dudhia, 2001: Coupling an advanced land-surface/hydrology model with the Penn State/NCAR MM5 modeling system. Part I: Model implementation and sensitivity. *Mon. Wea. Rev.*, **129**, 569–585.

Dudhia, J., 1989: Numerical study of convection observed during the winter monsoon experiment using a mesoscale two-dimensional model. *J. Atmos. Sci.*, **46**, 3077–3107.

Egger, J., 1990: Thermally induced flow in valleys with tributaries. Part I: Response to heating. *Meteorol. Atmos. Phys.*, **42**, 113–125.

Fujibe, F., 1999a: Climatology of apparent "sea breezes" associated with warm advection in the Kanto and the Tokachi-Konsen regions. *Tenki*, **46**, 501–512 (in Japanese).

Fujibe, F., K. Saito, D. S. Wratt, and S. G. Bradley, 1999b: A numerical study on the diurnal variation of low-level wind in the lee of a two-dimensional mountain. *J. Meteor. Soc. Japan*, **77**, 827–843.

Gaffin, D. M., 2007: Foehn winds that produced large temperature differences near the southern Appalachian Mountains. *Wea. Forecasting*, **22**, 145–159.

Groen, P., 1947: Note on the theory of nocturnal radiational cooling of the earth's surface. *J. Meteor.*, **4**, 63–66.

Grell, G. A., and D. Devenyi, 2002: A generalized approach to parameterizing convection combining ensemble and data assimilation techniques. *Geophys. Res. Lett.*, **29**, 38-1–38-4, doi:10.1029/2002GL015311.

Hayasaki, M., nd R. Kawamura, 2012: Cyclone activities in heavy rainfall episodes in Japan during Spring Season. *SOLA*, **8**, 45–48.

Iijima, Y., and M. Shinoda, 2002: The influence of seasonally varying atmospheric characteristics on the intensity of nocturnal cooling in a high mountain hollow. *J. Appl. Meteor*, **41**, 734–743.

Ikawa, M., and Y. Nagasawa, 1989: A numerical study of a dynamically induced foehn observed in the Abashiri-Ohmu area. *J. Meteor. Soc. Japan*, **67**, 429–458.

Inatsu, M., T. J. Yamada, T. Sato, K. Nakamura, N. Matsuoka, A. Komatsu, Y. N. Pokhrel, S. Sugimoto, and S. Miyazaki, 2012: A new project on development and application of comprehensive downscaling methods over Hokkaido. *EGU General Assembly Conference Abstracts*, **14**, 2551.

Ishizaki, N., and I. Takayabu, 2009: On the warming events over Toyama Plain by using NHRCM. *SOLA*, **5**, 129–132.

Kessler, E., 1969: *On the Distribution and Continuity of Water Substance in Atmospheric Circulation. Meteor. Monogr.,* **32**, 84 pp.

Kondo, J., 1983: On the unusual dryness and strong wind weather which caused a large number of forest fires over the Tohoku district on 27 April 1983 (Part 1). *Tenki*, **30**, 545–552 (in Japanese).

Kusaka, H., Y. Miya, and R. Ikeda, 2011: Effects of solar radiation amount and synoptic-scale wind on the local wind "Karakkaze" over the Kanto Plain in Japan. *J. Meteor. Soc. Japan*, **89**, 327–340.

Markowski, P., and Y. Richardson, 2010: *Mesoscale Meteorology in Midlatitudes, 1st Edition.*, Wiley-Blackwell, 407 pp.

Lin, Y. L., 2007: *Mesoscale Dynamics*. Cambridge University Press, 630 pp.

Matsushita, H., M. Matsuzaki, H. Nakamura, S. Ikeda, and Y. Ito, 2012: Seasonal change in conditions for occurrence of wet snow avalanches in Hokkaido. *Proceedings, 2012 International Snow Science Workshop*, Anchorage, Alaska, 878–883.

Mayr, G. J., L. Armi, A. Gohm, G. Zangl, D. R. Durran, C. Flamant, S. Gabersk, S. Mobbs, A. Ross, and M. Weissmann, 2007: Gap flows: Results from the Mesoscale Alpine Programme. *Quart. J. Roy. Meteor. Soc.*, **133**, 881–896.

Mlawer, E. J., S. J. Taubman, P. D. Brown, M. J. Iacono, and S. A. Clough, 1997: Radiative transfer for inhomogeneous atmospheres: RRTM, a validated correlated-k model for the longwave. *J. Geophys. Res.*, **102**, 16663–16682.

Monin, A. S., and A. M. Yaglom, 1975: *Statistical Fluid Mechanics*. Mechanics of Turbulence, Vol. 2. Dover Publications, Mineola, 882 pp.

Nakanishi, M., and H. Niino, 2004: An improved Mellor-Yamada level-3 model with condensation physics: Its design and verification. *Bound.-Layer Meteor.*, **112**, 1–31.

Nallapareddy, A., A. Shapiro, and J. J. Gourley, 2011: A climatology of nocturnal warming events associated with cold-frontal passages in Oklahoma. *J. Appl. Meteor. Climatol.*, **50**, 2042–2061.

Onogi, K., J. Tsutsui, H. Koide, M. Sakamoto, S. Kobayashi, H. Hatsushika, T. Matsumoto, N. Yamazaki, H. Kamahori, K. Takahashi, S. Kadokura, K. Wada, K. Kato, R. Oyama, T. Ose, N. Mannoji, and R. Taira, 2007: The JRA-25 Reanalysis. *J. Meteor. Soc. Japan*, **85**, 369–432.

Oard, M. J., 1993: A method for predicting chinook winds east of the Montana Rockies. *Wea. Forecasting*, **8**, 166–180.

Raphael, M. N., 2003: The Santa Ana winds of California. *Earth Interact.*, **7**, 1–13.

Reynolds, R. W., T. M. Smith, C. Liu, D. B. Chelton, K. S. Casey, and M. G. Schlax, 2007: Daily high-resolution-blended analysis for sea surface temperatures. *J. Climate*, **20**, 5473–5496.

Sato, T., and F. Kimura, 2003: A two-dimensional numerical study on diurnal cycle of mountain lee precipitation. *J. Atmos. Sci.*, **60**, 1992–2003.

Skamarock, W. C., J. B. Klemp, J. Dudhia, D. O. Gill, D. M. Barker, M. G. Duda, X.-Y. Huang, W. Wang, and J. G. Powers, 2008: *A Description of the Advanced Research WRF Version 3*. NCAR/TN-475+STR, 113 pp.

Takane, Y., and H. Kusaka, 2011: Formation mechanisms of the extreme high surface air temperature of 40.98 °C observed in the Tokyo metropolitan area: Considerations of dynamic foehn and foehnlike wind. *J. Appl. Meteor. Climatol.*, **50**, 1827–1841.

Tsunematsu, N., T. Sato, F. Kimura, K. Kai, Y. Kurosaki, T. Nagai, H. Zhou, and M. Mikami, 2005: Extensive dust outbreaks following the morning inversion breakup in the Taklimakan Desert. *J. Geophys. Res.*, **110**, D21207, doi:10.1029/2005JD005994.

Weissmann, M. D., G. J. Mayr, R. M. Banta, and A. Goem, 2004: Observations of the temporal evolution and spatial structure of the gap flow in the Wipp Valley on 2 and 3 October 1999. *Mon. Wea. Rev.*, **132**, 2684–2697.

White, L. D., 2009: Sudden nocturnal warming events in Mississippi. *J. Appl. Meteor. Climatol.*, **48**, 758–775.

Whiteman, C. D., X. Bian, and S. Zhong, 1999: Wintertime Evolution of the Temperature Inversion in the Colorado Plateau Basin. *J. App. Meteor.*, **38**, 1103–1117.

Zangl, G., 2003: Deep and shallow south foehn in the region of Innsbruck: Typical features and semi-idealized numerical simulations. *Meteor. Atmos. Phys.*, **83**, 237–261.